





Title	Doublet 1/2+ resonances of B9 in the complex scaling method
Author(s)	Odsuren, Myagmarjav; Myo, Takayuki; Kat , Kiyoshi
Citation	Physical Review C, 107(4), 044003 <a href="https://doi.org/10.1103/PhysRevC.107.044003">https://doi.org/10.1103/PhysRevC.107.044003</a>
Issue Date	2023-04-17
Doc URL	<a href="http://hdl.handle.net/2115/92178">http://hdl.handle.net/2115/92178</a>
Rights	©2023 American Physical Society
Type	article
File Information	PhysRevC.107.044003.pdf



[Instructions for use](#)

## Doublet $1/2^+$ resonances of ${}^9\text{B}$ in the complex scaling method

Myagmarjav Odsuren <sup>1,\*</sup>, Takayuki Myo<sup>2,3,†</sup> and Kiyoshi Katō <sup>4,‡</sup>

<sup>1</sup>*School of Engineering and Applied Sciences and Nuclear Research Center, National University of Mongolia, Ulaanbaatar 210646, Mongolia*

<sup>2</sup>*General Education, Faculty of Engineering, Osaka Institute of Technology, Osaka 535-8585, Japan*

<sup>3</sup>*Research Center for Nuclear Physics (RCNP), Osaka University, Ibaraki 567-0047, Japan*

<sup>4</sup>*Nuclear Reaction Data Centre, Faculty of Science, Hokkaido University, Sapporo 060-0810, Japan*



(Received 15 February 2023; accepted 4 April 2023; published 17 April 2023)

We try to resolve the longstanding controversy over the low-lying  $1/2^+$  state in  ${}^9\text{B}$ . Experimentally, the energies for this state show a gap between various measurements done by different groups and some of them reported that the existence of the state is unclear. The situation is similar in the theoretical calculations. We study the existence and structure of the  ${}^9\text{B}(1/2^+)$  state based on our previous method for the  $\alpha + \alpha + N$  cluster model with the complex scaling method that well explains the measured photodisintegration cross section for the  ${}^9\text{Be}(1/2^+)$ . We find two resonances at the energies of  $E_1^{\text{res}} = 1.81$  MeV with a decay width  $\Gamma = 1.98$  MeV and  $E_2^{\text{res}} = 2.38$  MeV,  $\Gamma = 1.81$  MeV in  ${}^9\text{B}$ . The charge radii and the three-body channel configurations are calculated to see the properties of two resonances. We also calculate the level density of two resonances, which indicates the difficulty to distinguish them in the energy distribution.

DOI: [10.1103/PhysRevC.107.044003](https://doi.org/10.1103/PhysRevC.107.044003)

### I. INTRODUCTION

The low-lying  $1/2^+$  states in the  ${}^9\text{Be}$  and  ${}^9\text{B}$  mirror nuclei have been studied with interests in nuclear structure theoretically and experimentally. However, we have not yet reached sufficient understanding. In  ${}^9\text{Be}$  [1], only the ground state is bound with a small binding energy ( $E = -1.57$  MeV measured from the  $\alpha + \alpha + n$  three-body threshold) and all the excited states are unbound. Thus,  ${}^9\text{Be}$  is a Borromean system of  $\alpha + \alpha + n$  having no-bound state of any two-body subsystem. In  ${}^9\text{B}$  [1], even the ground state is unbound and observed as a resonant state at 0.277 MeV measured from the  $\alpha + \alpha + p$  threshold (width  $\Gamma = 0.54 \pm 0.21$  keV). Such situations of  ${}^9\text{Be}$  and  ${}^9\text{B}$  nuclei seem to make it difficult to settle the excited states experimentally and theoretically. In particular, the low-lying  $1/2^+$  states bring about great difficulties due to the problems of the possible virtual states of an  $s$ -wave neutron in  ${}^9\text{Be}$  and broad resonance widths because of the low centrifugal barrier potential of low angular momenta.

The photodisintegration experiments [2,3] for  ${}^9\text{Be}$  show a shape peak just above the  ${}^8\text{Be} + n$  threshold, which suggests a resonant state [4]. However, the microscopic cluster model calculation by Arai *et al.* [5] could not identify the  $1/2^+$  resonance. Several years later, the same group [6] reported that the  $1/2^+$  state is a  ${}^8\text{Be}(0^+) + n$  virtual state based on the analytical continuation of the  $S$ -matrix method using the

${}^8\text{Be} + n$  and  ${}^5\text{He} + \alpha$  coupled channel model. Because an  $s$ -wave neutron in the two-body system has no resonance near the neutron threshold energy but a virtual state near the neutron threshold energy, we also investigated the  $1/2^+$  state of  ${}^9\text{Be}$  using a three-body model [7] of  $\alpha + \alpha + n$ , and showed that the observed photodisintegration cross section just above the  ${}^8\text{Be} + n$  threshold is well reproduced by the virtual state [8].

On the other hand, the  $1/2^+$  problem of the  ${}^9\text{B}$  nucleus seems to be more complicate due to no bound state in  ${}^9\text{B}$ . Many experiments [9–16] of the charge exchange reactions have been done to study low-lying states in  ${}^9\text{B}$ . However, there is an inconsistency among the reported excitation energies of the  $1/2^+$  state, ranging from  $E_{\text{ex}} = 1.16 \pm 0.05$  MeV by the  ${}^9\text{Be}({}^3\text{He}, t)$  reaction [13] to  $E_{\text{ex}} = 1.8 \pm 0.2$  MeV by the  ${}^{10}\text{B}({}^3\text{He}, \alpha)$  reaction [14]. But in some experiments [17,18], the  $1/2^+$  state around  $E_x \approx 1.6$ – $1.7$  MeV was not observed, and the location and existence of the excited state have been unclear. Theoretical results of the  $1/2^+$  state in  ${}^9\text{B}$  are also inconsistent [19]. The broad resonance in the  $1/2^+$  state was obtained in the coupled channel two-body calculation by Arai *et al.* [6], but Garrido *et al.* [4] reported the existence of two  $1/2^+$  resonance states around 2 MeV excitation energy by the  $\alpha + \alpha + p$  three-body calculation applying the adiabatic hyperspherical expansion method.

For the purpose to solve the  $1/2^+$  state problem in  ${}^9\text{Be}$  and  ${}^9\text{B}$ , in this paper we study the low-lying  $1/2^+$  state of  ${}^9\text{B}$  based on our previous methodology [7,8] for  ${}^9\text{Be}$ . The present calculations are performed by using the  $\alpha + \alpha + p$  three-body model with the orthogonality condition model (OCM) for the Pauli principle and the complex scaling method (CSM) for the correct boundary condition of resonant states.

\*odsuren@seas.num.edu.mn

†takayuki.myo@oit.ac.jp

‡kato-iku@gd6.so-net.ne.jp

We are facing two problems in calculations of the  $1/2^+$  resonance in  ${}^9\text{B}$ : One is how to identify a broad resonance solution accurately, and another is how to clarify the structure of the resonant state. For the first problem, we look for the stationary solution of the complex energy eigenvalue by drawing the  $b$  and  $\theta$  trajectories [20,21], where  $b$  and  $\theta$  are the parameters in the wave function, and then confirm the stable resonance solution, which can show a small expectation value of the radius in comparison with those of continuum solutions. For the second, we attempt two analyses to see the structures of the obtained resonances. One is the analytical continuation for the valence proton charge of the Coulomb interaction. It is expected from this result that we can clarify the relationship between the  ${}^9\text{B}$  and  ${}^9\text{Be}$  resonance solutions. Another is the calculation of channel amplitudes to see dominant components of configurations such as  ${}^8\text{Be} + p$  and  ${}^5\text{Li} + \alpha$  in the resonance solution.

From the results of these calculations and analyses, we conclude that two broad  $1/2^+$  resonances exist in  ${}^9\text{B}$  as pointed out by Garrido *et al.* [4]. Also, regarding the structures of the two  $1/2^+$  resonances, it is found that the first state has a mixed  ${}^8\text{Be} + p$  and  ${}^5\text{Li} + \alpha$  structure and the second state has a  ${}^5\text{Li} + \alpha$  structure. However, because these two  $1/2^+$  resonant states have a large overlap in the excitation energy due to small energy gap and broad widths of the resonances, we show that it is difficult to distinguish two resonant states in the energy distribution calculating the level density of two resonances.

In the next section, we briefly explain the present method for the  $\alpha + \alpha + p$  model and the complex scaling method. In Sec. III, we show two resonance solutions of the low-lying  $1/2^+$  states in  ${}^9\text{B}$ , and analyses of the analytical continuation of the valence nucleon charge and the channel amplitudes. In Sec. IV, discussions and a conclusion are given.

## II. METHOD

### A. Three-body model and complex scaling method

The Hamiltonian for the relative motion of the  $\alpha + \alpha + p$  three-body system is given as

$$\hat{H} = \sum_{i=1}^3 t_i - T_{\text{c.m.}} + \sum_{i=1}^2 V_{\alpha N}(\mathbf{r}_i) + V_{\alpha\alpha} + V_3 + V_{\text{PF}}, \quad (1)$$

where  $t_i$  and  $T_{\text{c.m.}}$  are kinetic energy operators for each particle and the center of mass of the system, respectively. The interactions between the valence nucleon and the  $i$ th  $\alpha$  particle is given as  $V_{\alpha N}(\mathbf{r}_i)$  [22], where  $\mathbf{r}_i$  is the relative coordinate between them. For  $V_{\alpha N}$ , we employ the Kanada-Kaneko-Nagata-Nomoto nuclear potential [22] in addition to the folding-type Coulomb interaction with the density of the  $s$ -wave  $\alpha$  particle. The explicit form of the  $\alpha - N$  Coulomb potential is expressed as

$$V_{\alpha N}^C(r_i) = \frac{Z_\alpha Z_N}{r_i} \text{erf}(\beta r_i), \quad (2)$$

where  $\beta = 0.5972 \text{ fm}^{-1}$ ,  $Z_\alpha = 2e$ , and  $Z_N = 1e$  (proton) and  $= 0e$  (neutron). For the  $\alpha - \alpha$  interaction  $V_{\alpha\alpha}$ , the folding potential of the effective  $NN$  [23] and the Coulomb interactions are used.

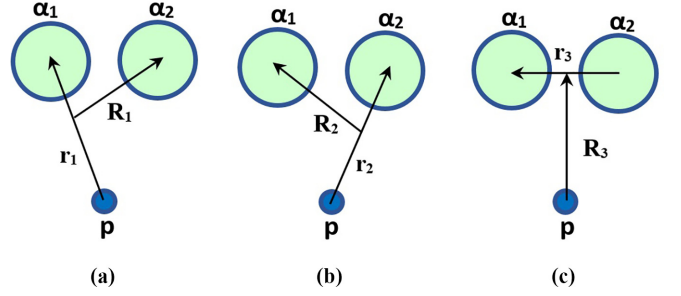


FIG. 1. Schematic illustration of three types of Jacobi coordinate sets of the  $\alpha + \alpha + p$  system. We call (a)–(c) sets as  $Y_a$ -,  $Y_b$ -, and  $T$ -coordinate systems, respectively.

As shown in [7], we introduce the three-cluster potential  $V_3$  to reproduce the binding energy of the  ${}^9\text{Be}$  ground state. The Pauli-forbidden states for  $\alpha + \alpha + N$ , which are the states having zero eigenvalues of the microscopic norm kernel, are projected out by using the pseudopotential  $V_{\text{PF}} = \lambda \{ |\Phi_{\text{PF}}^{\alpha\alpha}(\mathbf{r}_1)\rangle \langle \Phi_{\text{PF}}^{\alpha\alpha}(\mathbf{r}_1)| + |\Phi_{\text{PF}}^{\alpha N}(\mathbf{r}_2)\rangle \langle \Phi_{\text{PF}}^{\alpha N}(\mathbf{r}_2)| + |\Phi_{\text{PF}}^{\alpha N}(\mathbf{r}_3)\rangle \langle \Phi_{\text{PF}}^{\alpha N}(\mathbf{r}_3)| \}$  with a large repulsive strength ( $\lambda = 10^6$  MeV), where  $\Phi_{\text{PF}}^{\alpha\alpha}(\mathbf{r})$  and  $\Phi_{\text{PF}}^{\alpha N}(\mathbf{r})$  are the Pauli-forbidden states of  $\alpha + \alpha$  and  $\alpha + N$  systems, respectively.

The complex-scaled Schrödinger equation is expressed by using the complex-scaled Hamiltonian  $H^\theta$  as

$$H^\theta \Psi^J(\theta) = E^\theta \Psi^J(\theta). \quad (3)$$

We expand the three-body wave function  $\Psi^J(\theta)$  with spin  $J$  in the linear combination form of the different channels of the Jacobi coordinate systems as shown in Fig. 1. In the complex scaling, the relative coordinates of the three-body system of  $\alpha + \alpha + N$  are transformed as  $\mathbf{r}_i \rightarrow \mathbf{r}_i e^{i\theta}$  and  $\mathbf{R}_i \rightarrow \mathbf{R}_i e^{i\theta}$  with a real scaling angle  $\theta$ , where  $\mathbf{r}_i$  and  $\mathbf{R}_i$  ( $i = 1, 2, 3$ ) are the Jacobi coordinates shown in Fig. 1. Solving the complex-scaled Schrödinger equation with appropriate  $L^2$ -basis functions, we obtain the energy eigenvalues and eigenstates [21]. In this calculations, we employ the Gaussian functions with different size parameters  $b$  as the basis functions for each relative motion of the  $Y$ - and  $T$ -type Jacobi coordinate systems [7,8].

### B. Channel amplitudes of resonance solutions in the $\alpha + \alpha + p$ model

The wave function of the  ${}^9\text{B} = \alpha + \alpha + p$  system is expressed as a sum of  $Y$ - and  $T$ -coordinate basis functions:

$$\Psi_k^J(\theta) = \sum_{iy} C_{iy}^k(\theta) |\Phi_{iy}^Y\rangle + \sum_{ir} C_{ir}^k(\theta) |\Phi_{ir}^T\rangle, \quad (4)$$

where the basis state  $\Phi_{iy(c)}^Y$  is symmetrized with respect to the exchange of  $\alpha$  particles and given as

$$\Phi_{iy(c)}^Y = \frac{1}{\sqrt{2}} \{ \Phi_{iy(c)}^{Y_a} + \Phi_{iy(c)}^{Y_b} \}. \quad (5)$$

The wave function  $\Phi_{iy(c)}^Y$  describes an  $i$ th basis state of the channel  $c = (\ell_1, \ell_2, \ell)$  in the  ${}^5\text{Li}(\alpha + p) + \alpha$  configuration, where  $\ell_1$  and  $\ell_2$  are the orbital angular momenta between  $\alpha$  and  $p$  in  ${}^5\text{Li}$  and between  ${}^5\text{Li}$  and  $\alpha$ , respectively, for the

total orbital angular momentum  $\ell = [\ell_1 \otimes \ell_2]$ . On the other hand, the channel in the  $T$ -coordinate  ${}^8\text{Be}(\alpha + \alpha) + p$  system is also described as  $c = (\ell_1, \ell_2, \ell)$ , where  $\ell_1$  and  $\ell_2$  are the orbital angular momenta between two  $\alpha$  clusters in  ${}^8\text{Be}$  and between  ${}^8\text{Be}$  and  $p$ , respectively, for the total orbital angular momentum  $\ell = [\ell_1 \otimes \ell_2]$ . We take into account the spin coupling of a valence nucleon to the total spin  $J = [1/2 \otimes \ell]$ . Radial components of each relative wave function are expanded using the Gaussian basis functions [24]. The number of the basis functions is determined to reach the convergence of the numerical results and we employ 23 Gaussian functions for each coordinate and the range of the Gaussian is taken from 0.15 fm to 60 fm. In Eq. (4), the coefficients  $C_{i_Y}^k(\theta)$  and  $C_{i_T}^k(\theta)$  are obtained by solving the complex-scaled equation in Eq. (3) for the index  $k$  of eigenstates.

To calculate the channel amplitudes of  ${}^8\text{Be} + p$  and  ${}^5\text{Li} + \alpha$  in the eigenstates  $k$ , we introduce two kinds of the projection operators:

$$\hat{P}_c^Y = \sum_{i_Y(c)} |\Phi_{i_Y(c)}^{Y_a}\rangle \langle \Phi_{i_Y(c)}^{Y_a}|, \quad (6)$$

$$\hat{P}_c^T = \sum_{i_T(c)} |\Phi_{i_T(c)}^T\rangle \langle \Phi_{i_T(c)}^T|, \quad (7)$$

where  $i_Y(c)$  ( $i_T(c)$ ) means to sum over  $i_Y$  ( $i_T$ ) fixing the channel  $c$ .

Using the projection operators, we define the corresponding channel amplitudes of the wave function  $\Psi_k^J(\theta)$  as

$$\begin{aligned} Z_c^Y(k) &= \langle \Psi_k^J | \hat{P}_c^Y | \Psi_k^J \rangle, \\ Z_c^T(k) &= \langle \Psi_k^J | \hat{P}_c^T | \Psi_k^J \rangle. \end{aligned} \quad (8)$$

It should be noticed here that the sum of these amplitudes is not unity because the channel wave functions in Eq. (4) are not orthogonal with each other. However, it is meaningful to see the contributions of the specific channel of the  $Y$ - and  $T$ -coordinate systems in the state  $\Psi_k^J$ .

### III. RESULTS

#### A. The low-lying excited $1/2^+$ states in ${}^9\text{B}$

Using the same Hamiltonian used for  ${}^9\text{Be}$  and the Coulomb potential between proton and  $2\alpha$ , we obtain the  ${}^9\text{B}(3/2^-)$  ground state energy of 0.277 MeV measured from the  $\alpha + \alpha + p$  threshold energy, with the decay width  $1.73 \times 10^{-3}$  MeV, which agree well with the observed 0.277 MeV and  $0.54 \times 10^{-3}$  MeV [1], respectively. In Fig. 2, we show the distribution of complex energy eigenvalues for the  ${}^9\text{B}(1/2^+)$  state, solving the complex-scaled Schrödinger equation Eq. (3) with the scaling angle  $\theta = 20^\circ$ .

We find two resonances at energies  $E_1^{\text{res}} = 1.81$  MeV and  $E_2^{\text{res}} = 2.38$  MeV with decay widths  $\Gamma_1 = 1.98$  MeV and  $\Gamma_2 = 1.81$  MeV, respectively. The first and second resonances are represented by filled and open triangles in Fig. 2, respectively. The result of these two resonances also supports the report of Garrido *et al.* [4]. In addition to the resonance solutions,  $\alpha + \alpha + p$  three-body continuum (double line),  ${}^8\text{Be}(0^+) + p$  (solid line),  ${}^5\text{Li}(3/2^-) + \alpha$  (dashed-dotted line), and  ${}^8\text{Be}(2^+) + p$  (dotted-line) two-body continuum solutions are obtained separately. As shown in Fig. 2, the first resonance

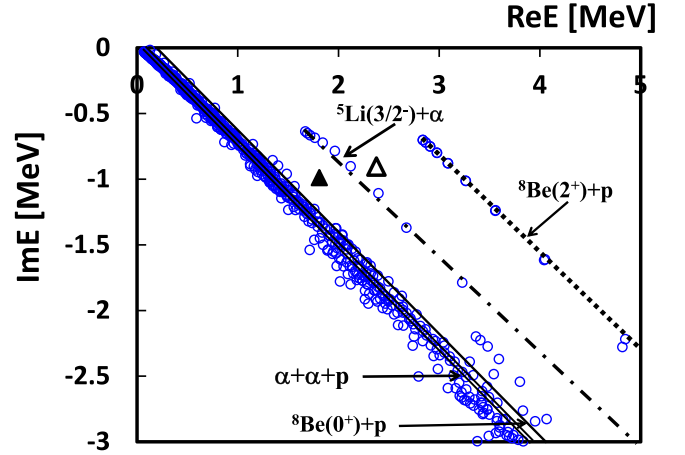


FIG. 2. Distribution of energy eigenvalues of the  ${}^9\text{B}(1/2^+)$  state obtained by using the complex scaling with  $\theta = 20^\circ$ . Open and filled triangles show the resonance states. The continuum states of the three- and two-body subsystems are given by double, solid, dashed-dotted, and dotted black lines.

state is located in between the two-body continuum states of  ${}^8\text{Be}(0^+) + p$  and  ${}^5\text{Li} + \alpha$  and the second resonance state is located at an energy between the two-body continuum states of  ${}^5\text{Li}(3/2^-) + \alpha$  and  ${}^8\text{Be}(2^+) + p$ . It should be noted that we have confirmed that the first and second resonances take a stationary solution of eigenenergies by performing  $b$  and  $\theta$  trajectories in the complex scaling method [20,21].

We can confirm that the resonance solutions are well separated from the continuum solutions and also distinguished by calculating the expectation values of the root-mean-square charge radius. As discussed in Ref. [26], the expectation values of the radius are given by complex numbers for resonance and continuum solutions in CSM. When the imaginary part is smaller than the real part, the real part value is expected to describe the physical character of the corresponding state. In Tables I and II, we show the calculated expectation values of the charge radius for several solutions around the first and

TABLE I. Calculated eigenenergies (ReE, ImE), and charge radius (ReR, ImR) of the first resonance (fourth state, R) of  ${}^9\text{B}(1/2^+)$  with its neighboring continuum solutions (C) for the valence proton charge at  $1.0e$ . Angle indicates the argument of the eigenvalue in the complex energy plane.

type	Eigenenergies		Angle $\varphi$ [deg]	Charge radius	
	ReE [MeV]	ImE [MeV]		ReR [fm]	ImR [fm]
C	1.789	-1.323	36.49	25.600	9.593
C	1.793	-1.362	37.22	31.245	17.814
C	1.806	-1.328	36.33	23.514	8.347
R	1.810	-0.989	28.65	8.672	5.011
C	1.815	-1.445	38.59	61.120	22.421
C	1.818	-1.327	36.13	23.697	8.820
C	1.838	-1.407	37.43	22.302	9.744

TABLE II. The same results in Table I, but for the second resonance of the  ${}^9\text{B}(1/2^+)$  state. The fourth state is a resonance.

type	Eigenenergies		Angle $\varphi$ [deg]	Charge radius	
	Re $E$ [MeV]	Im $E$ [MeV]		Re $R$ [fm]	Im $R$ [fm]
C	2.354	-1.789	37.23	76.635	40.004
C	2.358	-1.844	38.02	39.662	12.751
C	2.371	-1.916	38.94	37.367	7.556
R	2.377	-0.904	20.82	7.865	3.746
C	2.379	-1.845	37.80	15.389	10.378
C	2.380	-1.932	38.99	46.689	20.415
C	2.389	-1.734	35.96	19.354	7.073

second resonances. The calculated eigenenergies of the real (Re $E$ ) and imaginary (Im $E$ ) parts are also presented together with the angle  $[\varphi = \tan^{-1}(\text{Im}E/\text{Re}E)]$  on the complex energy plane.

The angle  $\varphi$  of the resonance solution is smaller than  $2\theta = 40$  degrees, while continuum solutions distribute along  $2\theta$  line. In Tables I and II, we marked resonance and continuum solutions with  $R$  and  $C$ , respectively. From the results of the charge radius, we can also confirm that the resonance solutions have smaller values of Re $R$  and Im $R$  in comparison with those of continuum solutions. For second resonance, although the resonance energy is higher than the first resonance, this resonance seems to be stable because the resonance width, the imaginary part of the charge radius and the angle  $\varphi$  are smaller than those of the first resonance.

We also calculate the  ${}^9\text{B}(1/2^+)$  state without three-body potential  $V_3$  ( $v_3 = 0$  in Eq. (6) of Ref. [7]), and obtain for the first and second resonances  $E_1^{\text{res}} = 1.88$  MeV with a decay width  $\Gamma_1 = 2.28$  MeV and  $E_2^{\text{res}} = 2.56$  MeV with  $\Gamma_2 = 1.66$  MeV, respectively. These results imply that the calculated two  $1/2^+$  resonances of  ${}^9\text{B}$  have a weak dependence on the three-body potential [4]. The reason for this would come from a spatially extended two-body cluster configuration but not a compact three-body configuration.

### B. Structures of the $1/2^+$ resonances

Here, we focus on the properties of the obtained two  $1/2^+$  resonances in  ${}^9\text{B}$  based on two results of calculations.

First, to see the relationship between the  $1/2^+$  states in  ${}^9\text{Be}$  and  ${}^9\text{B}$ , we calculate  $1/2^+$  resonances by gradually reducing the charge of the valence proton. In the present calculation, the  ${}^9\text{Be}$  and  ${}^9\text{B}$  systems are described with the same Hamiltonian except for the Coulomb interaction between valence proton and two  $\alpha$ 's. The Coulomb interaction  $V_{\alpha N}^C$  expressed by Eq. (2) works in  ${}^9\text{B}$  with  $Z_N = 1e$  for  $N = \text{proton}$ , but does not in  ${}^9\text{Be}$  with  $Z_N = 0e$  for  $N = \text{neutron}$ . Reducing  $Z_N$  from  $1e$  to zero, we can see  $1/2^+$  resonances how to be changed from  ${}^9\text{B}$  to  ${}^9\text{Be}$ .

Figure 3 shows the analytical continuation for the valence proton charge in the Coulomb interaction. The open circles show the calculated eigenvalues of the  $1/2^+$  continuum solutions of  ${}^9\text{Be}$ . The filled triangles show the energy

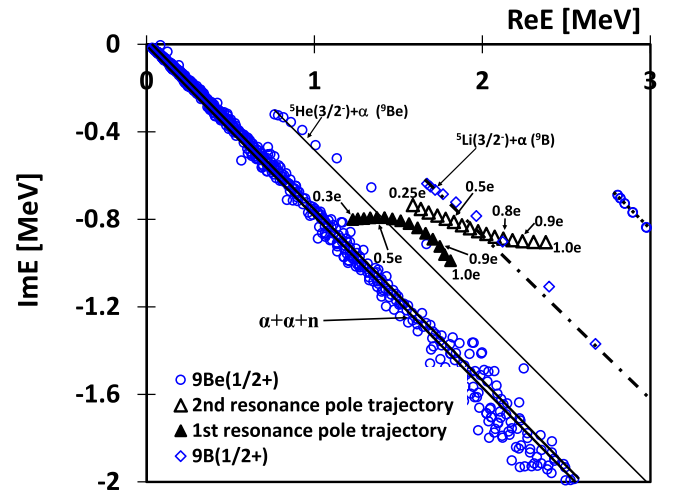


FIG. 3. Analytical continuation of pole trajectories obtained by decreasing the point charge of a valence proton for the first (filled triangles) and second (open triangles) resonance states in  ${}^9\text{B}(1/2^+)$ . The open blue circles are the distribution of the eigenvalues of the  ${}^9\text{Be}(1/2^+)$  state. The open diamonds present the  ${}^5\text{Li} + \alpha$  continuum solutions for  ${}^9\text{B}$ .  $\theta = 20^\circ$  is used.

eigenvalues of the first resonance obtained by reducing the point charge of the valence proton to 70 percent ( $Z_N = 0.3e$ ). The open triangles show the energy eigenvalues of the second resonance in the same way as the first resonance, but to 75 percent ( $0.25e$ ) of  ${}^9\text{B}(1/2^+)$ . Below 70 percent for the first and 75 percent for the second states, the  $1/2^+$  state solutions could not be evaluated by the analytical continuation for the valence proton charge to  $0e$ , because resonance eigenvalues cannot be well separated from three-body and two-body continuum solutions.

From Fig. 3, the first resonance solution seems to approach to the  $2\theta$  lines of  ${}^8\text{Be} + n$  and  $\alpha + \alpha + n$  continua, which are almost degenerated energetically. On the other hand, the second one comes closer to the  $2\theta$  line of  ${}^5\text{He}(3/2^-) + \alpha$  continuum. Thus, we suppose that two isolated resonances of the  $1/2^+$  states in  ${}^9\text{B}$  are absorbed into the continuum solutions and disappear when  $Z_n \rightarrow 0e$  in  ${}^9\text{Be}$ . This is consistent with no-resonance result of the previous calculations [5,7,8] of  ${}^9\text{Be}$ .

Next, to see the structures of the two  $1/2^+$  resonances, we calculate the channel amplitudes  $Z_c^Y(k)$  and  $Z_c^T(k)$  of Eq. (8) for five and three channels of  $Y$  [ $(\alpha + p) + \alpha$ ] and  $T$  [ $(\alpha + \alpha) + p$ ] configurations, respectively. In the  $Y$  configuration of  ${}^5\text{Li} + \alpha$ , the  ${}^5\text{Li}$  cluster is described by  $p$  and  $sd$  orbits of the proton around the  $\alpha$  core, which correspond to  $\ell = 0$  ( $s$ ),  $1$  ( $p$ ), and  $2$  ( $d$ ) and these states make five channels ( $Y_1 - Y_5$ ) for the total spin-parity  $J^\pi = 1/2^+$ . Similarly, in the  $T$  configuration of  ${}^8\text{Be} + p$ , the  ${}^8\text{Be}$  cluster is described by the  $0^+$  and  $2^+$  rotational wave functions of the  $\alpha + \alpha$  dumbbell, which correspond to  $\ell = 0$  and  $2$  and make three channels described by  $T_1$ ,  $T_2$ , and  $T_3$ .

The obtained channel amplitudes for the first and second resonances are presented in Tables III and IV, respectively. Although the channel amplitudes of resonances are given by complex numbers, the real parts are larger than the imaginary



TABLE III. The channel amplitudes  $Z_c^Y(k)$  and  $Z_c^T(k)$  of the first resonance of  ${}^9\text{B}(1/2^+)$ .

Configuration	$\ell_1, \ell_2, \ell$	Channel amplitude	
		Re	Im
$Y_1$	1,1,0	0.4529	-0.2846
$Y_2$	1,1,1	-0.0016	-0.0406
$Y_3$	0,0,0	0.7199	0.2468
$Y_4$	2,2,0	0.0784	0.0703
$Y_5$	2,2,1	-0.0025	-0.0204
$T_1$	0,0,0	1.0014	0.1173
$T_2$	2,2,0	-0.0394	-0.0981
$T_3$	2,2,1	-0.0010	-0.0302

ones and we discuss the properties of channel amplitudes by seeing their real parts.

From Table III for the first  $1/2^+$  resonance, we see that the  $T_1$  configuration of  $(\ell_1, \ell_2, \ell)=(0,0,0)$  has the largest amplitude (1.0014 +  $i$ 0.1173) compared to the other channel amplitudes. This means that the first  $1/2^+$  resonance has a  ${}^8\text{Be}(0^+) + p$  configuration dominantly, and it is consistent with the analytical continuation behavior of the first resonance. However, the channel amplitudes of  $Y_3$  and  $Y_1$  are not small. Such results suggest that the first  $1/2^+$  resonance has a strong mixing of  ${}^8\text{Be}(0^+) + p$  and  ${}^5\text{Li} + \alpha$  configurations. The  $Y_3$  configuration, having the secondly largest channel amplitude, consists of an  $1s$ -shell proton configuration in the  ${}^5\text{Li}$  cluster.

The channel amplitudes  $Z_c^Y(k)$  and  $Z_c^T(k)$  of the second  $1/2^+$  resonance are shown in Table IV, and the dominant amplitude is seen in the  $Y_1$  configuration with a  $p$ -wave proton in  ${}^5\text{Li}$ . This result is also consistent with the analytical continuation of the second resonance presented in Fig. 3. Thus, the second  $1/2^+$  resonance is considered to have the  ${}^5\text{Li}(3/2^-) + \alpha$  configuration dominantly.

#### IV. DISCUSSIONS AND CONCLUSION

According to our previous studies [7,8], the  $1/2^+$  state of  ${}^9\text{Be}$  is a virtual state of the  $s$ -wave neutron around the  ${}^8\text{Be}(0^+)$  cluster. However, we obtain two  $1/2^+$  resonances for  ${}^9\text{B}$  using the same Hamiltonian as used for  ${}^9\text{Be}$  and the

 TABLE IV. The same results in Table III, but for the second resonance of  ${}^9\text{B}(1/2^+)$ .

Configuration	$\ell_1, \ell_2, \ell$	Channel amplitude	
		Re	Im
$Y_1$	1,1,0	1.0033	0.1629
$Y_2$	1,1,1	0.2334	0.0221
$Y_3$	0,0,0	-0.1821	-0.0308
$Y_4$	2,2,0	0.098	-0.1924
$Y_5$	2,2,1	0.0731	-0.0119
$T_1$	0,0,0	0.2266	0.0422
$T_2$	2,2,0	0.3860	-0.0976
$T_3$	2,2,1	0.1209	-0.0138

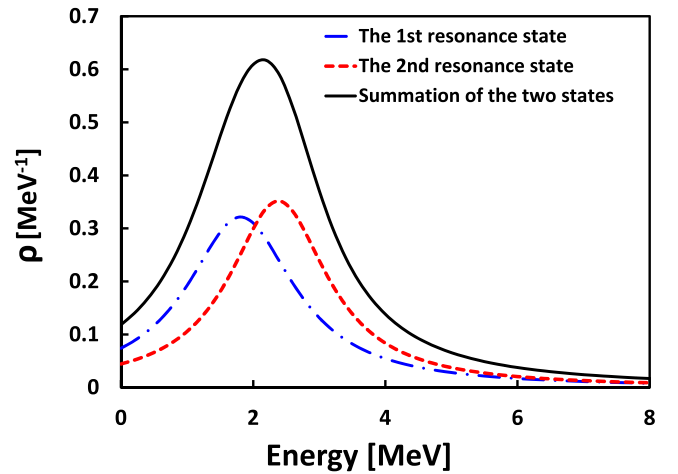


FIG. 4. The calculated level density of the two resonances of  ${}^9\text{B}(1/2^+)$  measured from the  $\alpha + \alpha + p$  threshold energy. The dotted-dashed line is the contribution of the first broad resonance state, the dashed line is the contribution of the second resonance state, and the solid line is the sum of the two resonance states.

Coulomb potential of the valence proton. This is considered as an indication of the mirror symmetry breaking due to the Coulomb interaction on the valence nucleon in  ${}^9\text{Be}$  and  ${}^9\text{B}$ .

The long-range Coulomb potential acts as a barrier that confines the  $s$ -wave proton around the  ${}^8\text{Be}(2\alpha)$  cluster. As a result, this Coulomb potential barrier causes  ${}^9\text{B}$  to have two  $1/2^+$  resonances. The first  $1/2^+$  resonance in  ${}^9\text{B}$  appears as an  $\alpha + \alpha + p$  three-body state with mixed configurations of  ${}^8\text{Be} + p$  and  ${}^5\text{Li} + \alpha$ . The mixing of the  ${}^5\text{Li} + \alpha$  configuration is also due to the open  ${}^5\text{Li} - \alpha$  threshold in  ${}^9\text{B}$  as shown in Fig. 2, unlike that of  ${}^9\text{Be}$ . Furthermore, the  ${}^5\text{Li} + \alpha$  configuration dominates at the second resonance in  ${}^9\text{B}$ , which does not exist in  ${}^9\text{Be}$ .

Finally, we consider the observability of the two resonances in  ${}^9\text{B}$ , because the positions of the two resonances are close to each other. For this purpose, we calculate the level density [21,25] of the  $1/2^+$  resonances:

$$\rho(E) = \delta(E - E_1) + \delta(E - E_2) = \rho_1(E) + \rho_2(E), \quad (9)$$

where  $E_i = E_i^{\text{res}} - i\Gamma_i/2$  and

$$\rho_i(E) = -\frac{1}{\pi} \text{Im} \frac{1}{E - E_i^{\text{res}} + i\Gamma_i/2}. \quad (10)$$

In Fig. 4, we show the calculated level densities of the first and second resonances,  $\rho_1(E)$  and  $\rho_2(E)$ , respectively, and the sum  $[\rho(E)]$  of them. We see that the level densities of the two resonances largely overlap and then it become difficult to distinguish these states in the observation.

In conclusion, we confirmed two resonances of  ${}^9\text{B}(1/2^+)$  at the energies  $E^{\text{res}} = 1.81$  MeV with a decay width  $\Gamma = 1.98$  MeV and  $E^{\text{res}} = 2.38$  MeV,  $\Gamma = 1.81$  MeV. The present results are consistent with the results in Ref. [4], which first demonstrated two resonances, but our calculated energies are slightly different from those in Ref. [4]. Garrido *et al.* [4] calculated two  $1/2^+$  resonances at  $(E^{\text{res}}, \Gamma) = (2 \text{ MeV},$

1.3 MeV) and (2.05 MeV, 1.6 MeV). The energy difference between two resonances is 0.05 MeV, which is smaller than our case (0.57 MeV). These resonances are calculated to have large widths, though our results are a little bit larger than those in Ref. [4], in both the cases. The first resonance shows a two-body  ${}^8\text{Be} + p$  structure in the result in Ref. [4], but a mixed structure of  ${}^8\text{Be} + p$  and  ${}^5\text{Li} + \alpha$  configurations in our result. The second resonance is commonly predicted to have a  ${}^5\text{Li} + \alpha$  cluster structure in both calculations.

From the level density calculations of two resonances, we confirm that two resonances largely overlap due to their close resonance energies and wide decay widths. Therefore, it is

difficult to observe low-lying two  $1/2^+$  resonances separately in  ${}^9\text{B}$ .

#### ACKNOWLEDGMENT

This work was supported by JSPS KAKENHI Grants No. 18K03660, 20K03962, and 22K03643 and the National University of Mongolia's Support for High Impact Research program no. P2022-4378. Numerical calculations were partly achieved through the use of the program made by Y. Kikuchi and the server at the Nuclear Research Center, National University of Mongolia.

- 
- [1] D. Tilley, J. Kelley, J. Godwin, D. Millener, J. Purcell, C. Sheu, and H. Weller, *Nucl. Phys. A* **745**, 155 (2004).
  - [2] C. W. Arnold, T. B. Clegg, C. Iliadis, H. J. Karwowski, G. C. Rich, J. R. Tompkins, and C. R. Howell, *Phys. Rev. C* **85**, 044605 (2012).
  - [3] H. Utsunomiya, S. Katayama, I. Gheorghe, S. Imai, H. Yamaguchi, D. Kahl, Y. Sakaguchi, T. Shima, K. Takahisa, and S. Miyamoto, *Phys. Rev. C* **92**, 064323 (2015).
  - [4] E. Garrido, D. V. Fedorov, and A. S. Jensen, *Phys. Lett. B* **684**, 132 (2010).
  - [5] K. Arai, Y. Ogawa, Y. Suzuki, and K. Varga, *Phys. Rev. C* **54**, 132 (1996).
  - [6] K. Arai, P. Descouvemont, D. Baye, and W. N. Catford, *Phys. Rev. C* **68**, 014310 (2003).
  - [7] M. Odsuren, Y. Kikuchi, T. Myo, M. Aikawa, and K. Katō, *Phys. Rev. C* **92**, 014322 (2015).
  - [8] Y. Kikuchi, M. Odsuren, T. Myo, and K. Katō, *Phys. Rev. C* **93**, 054605 (2016).
  - [9] J. B. Marion, T. W. Bonner, and C. F. Cook, *Phys. Rev.* **100**, 91 (1955).
  - [10] R. J. Slobodrian, H. Bichel, J. S. C. McKee, and W. F. Tivol, *Phys. Rev. Lett.* **19**, 595 (1967).
  - [11] J.-C. Chou, C.-M. Fou, C.-S. Lin, P.-S. Song, M. Wen, and Y.-C. Liu, *J. Phys. Soc. Jpn.* **44**, 1 (1978).
  - [12] M. Burlein, H. T. Fortune, P. H. Kutt, R. Gilman, R. Sherr, and J. D. Brown, *Phys. Rev. C* **38**, 2078 (1988).
  - [13] K. Kadija, G. Paic, B. Antolkovic, A. Djaloic, and J. Bojowald, *Phys. Rev. C* **36**, 1269 (1987).
  - [14] N. Arena, S. Cavallaro, G. Fazio, G. Giardina, A. Italiano, and F. Mezzanares, *Europhys. Lett.* **5**, 517 (1988).
  - [15] W. N. Catford, L. K. Fifield, E. L. Reber, K. W. Kemper, and J. D. Brown, *Nucl. Phys. A* **550**, 517 (1992).
  - [16] M. A. Tiede, K. W. Kemper, N. R. Fletcher, D. Robson, D. D. Caussyn, S. J. Bennett, J. D. Brown, W. N. Catford, C. D. Jones, D. L. Watson, and W. D. M. Rae, *Phys. Rev. C* **52**, 1315 (1995).
  - [17] R. W. Bauer, J. D. Anderson, and C. Wong, *Nucl. Phys.* **56**, 117 (1964).
  - [18] H. Ueno, T. Nakagawa, M. Baba, J. Kasagi, H. Orihara, and T. Tohei, *J. Phys. Soc. Jpn.* **40**, 1537 (1976).
  - [19] F. C. Barker, *Phys. Rev. C* **53**, 2539 (1996).
  - [20] S. Aoyama, T. Myo, K. Katō, and K. Ikeda, *Prog. Theor. Phys.* **116**, 1 (2006).
  - [21] T. Myo, Y. Kikuchi, H. Masui, and K. Katō, *Prog. Part. Nucl. Phys.* **79**, 1 (2014).
  - [22] H. Kanada, T. Kaneko, S. Nagata, and M. Nomoto, *Prog. Theor. Phys.* **61**, 1327 (1979).
  - [23] E. W. Schmid and K. Wildermuth, *Nucl. Phys. A* **26**, 463 (1961).
  - [24] E. Hiyama, Y. Kino, and M. Kamimura, *Prog. Part. Nucl. Phys.* **51**, 223 (2003).
  - [25] M. Odsuren, K. Katō, M. Aikawa, and T. Myo, *Phys. Rev. C* **89**, 034322 (2014).
  - [26] T. Myo and K. Katō, *Phys. Rev. C* **107**, 014301 (2023).